Tom Gaisser Venice 25-2-99

Antiprotons at solar maximum

– "primary" vs. "secondary" $\bar{p}$

"Secondary" $\bar{p}$ from $p\,H \to p\bar{p}NN\ldots$ in ISM

High threshold ($E_{Lab} > 7m_p$)

+ steep primary spectrum

$\Rightarrow$ peak in secondary $\bar{p}$ spectrum

$\sim E_{kin} \sim 2$ GeV

"primary" $\bar{p}$ have softer spectra $E_{kin} \lesssim 1$ GeV

Secondary $\bar{p}/cm^3 \sim \tau\, Q_{\bar{p}}\ (cm^{-3}s^{-1})$

$$\phi_{\bar{p}}(E) \sim \beta c\, n_H \frac{\tau_{esc}}{1+\tau_{esc}/\tau_{\bar{p}}} \int_{E_{min}>E}^{\infty} dE' \left\{ \phi_p(E')\, 2\, \frac{d\sigma_{pH\to\bar{p}}}{dE} + \phi_{\bar{p}}(E') \left[\frac{d\sigma_{\bar{p}H\to\bar{p}}}{dE} + \frac{d\sigma_{\bar{p}H\to\bar{n}}}{dE} \right] \right\}$$

$\bar{p}$ flux in ISM

Work with

John Bieber + Adri Burgen

(solar modulation experts)

+ Ralph Engel, TKG, Stefan Roesler

Todor Stanev

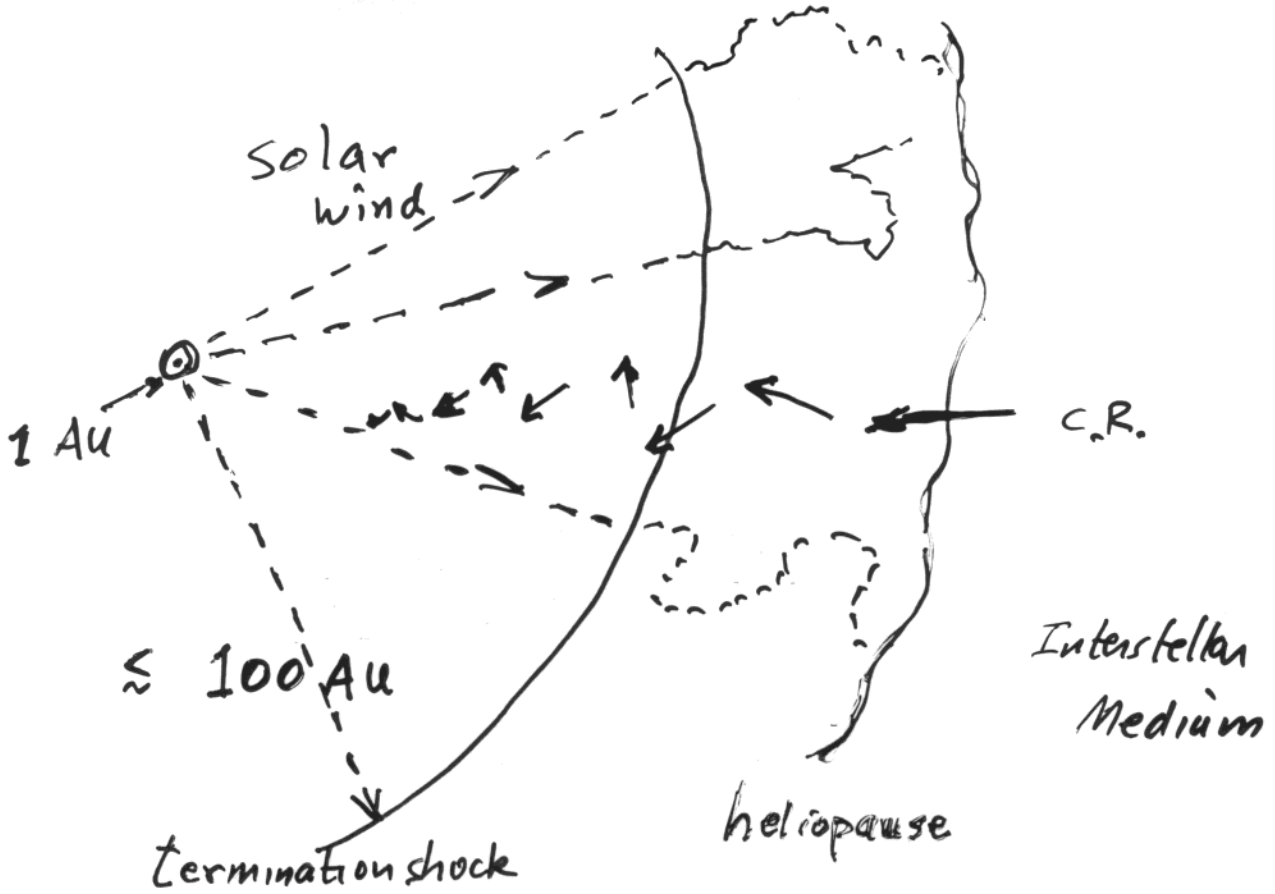

A cosmic ray entering heliosphere loses energy.

Particles with $E \lesssim 200$ MeV (in ISM) are practically excluded during strong solar activity because outward convection dominates diffusion inward.

Effect is greatest during periods of high solar magnetic activity because magnetic turbulence couples to the CR particles

interstellar

modulation of primary p

LEAP (or $\bar{p}$?)

E-S. Seo et al.

Ap. J. 1991

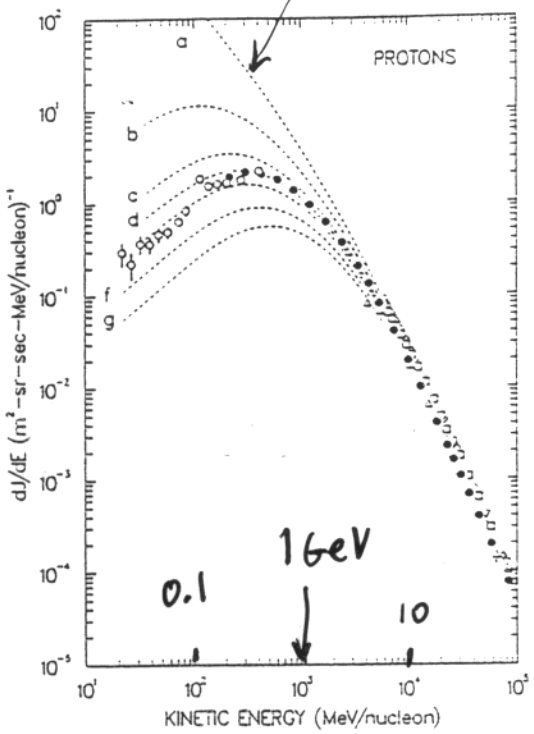

FIG. 9a

FIG. 9.—Differential energy spectra for cosmic-ray protons (*a*) and helium nuclei (*b*) mea the previous balloon measurements: *open diamonds* (1976 data), *open squares*. (1979 data), W Smith et al. (1973). The dashed curves represent the local intersteilar and modulated spec parameter ϕ: a, local interstellar spectra (no modulation); b, ϕ = 200 MV; c, ϕ = 400 MV; d

secondary $\bar{p}$:

$p + gas \rightarrow p\, N\, p\, \bar{p} + \cdots$

in ISM

modulation of secondary $\bar{p}$

$$\langle y_{\bar{p}}(E)\rangle = N_H m_p V \tau_{\bar{p}} ,$$

we obtain for the equilibrium differential flux of antiprotons

$$\frac{dN_{\bar{p}}(\bar{E})}{d\bar{E}} = \frac{2\langle y_{\bar{p}}(\bar{E})\rangle}{m_p}\int_{\bar{E}}^{\infty}\frac{d\sigma_{\bar{p}}}{d\bar{E}}(\bar{E},E)\frac{dN_0}{dE}\,dE, \qquad (5)$$

where

$$\langle y_{\bar{p}}(E)\rangle = [\langle y_p(E)\rangle^{-1} + \langle y_A(E)\rangle^{-1}]^{-1} . \qquad (6)$$

$\langle y_p(E)\rangle$ is the mean matter traversed by cosmic-ray protons and $\langle y_A(E)\rangle$ is the mean path for $\bar{p}p$ annihilation. $\langle y_p(E)\rangle$ is generally thought to be of the order of 3 to 6 g/cm² when E is of the order of a few GeV; by contrast $\langle y_A(E)\rangle$ in the same energy range is found, from accelerator data,[8] to be 30 to 50 g/cm² so that annihilation reduces the $\bar{p}$ flux by 10 or 15 percent at several GeV of kinetic energy. At very low energies (a few hundred MeV) the reduction can be as large as a factor of two; for the present this is of only academic interest. In Fig. 1 we have plotted the interstellar antiproton flux on the assumption that $\langle y_{\bar{p}}(\bar{E})\rangle = 5$ g/cm² over the entire energy range. The flux to be expected on the basis of some other form for

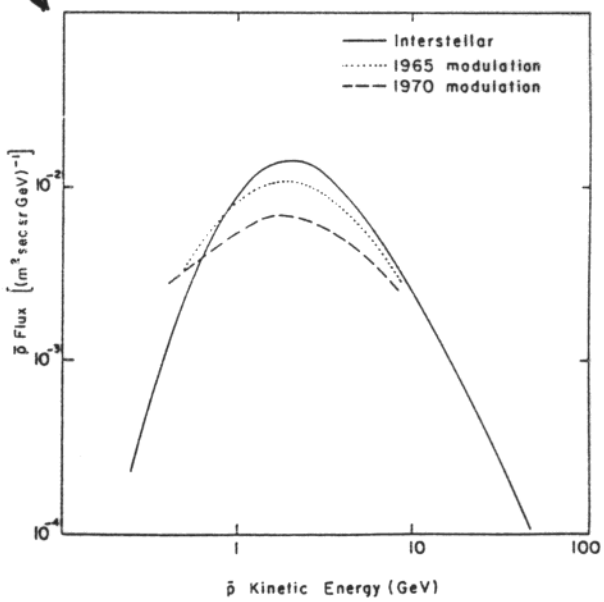

FIG. 1. Equilibrium differential $\bar{p}$ flux expected to be produced by the observed primary-proton spectrum if cosmic rays traverse an average of 5 g/cm² of matter during their confinement to the galaxy.

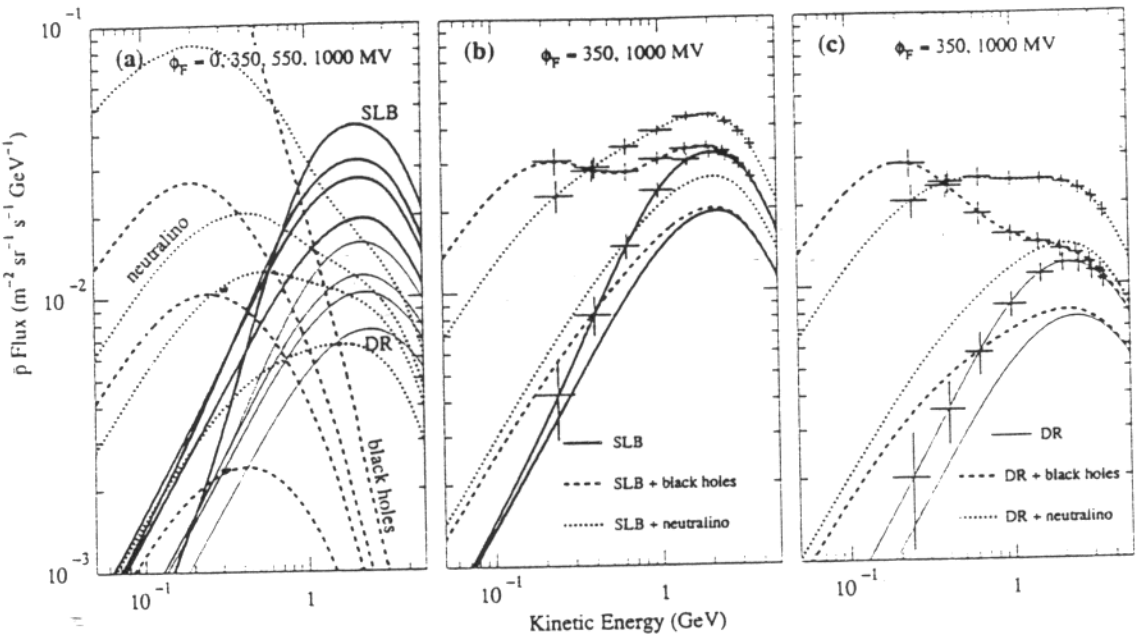

Fig. 2. (a) The expected energy spectra of $\bar{p}$'s from evaporating PBHs with $\mathcal{R} = 5 \times 10^{-3}$ $pc^{-3}yr^{-1}$ (dashed lines) and from the neutralino annihilation for the case #1 with $\xi = 25$ (dotted lines), as well as the secondary $\bar{p}$'s in the SLB (thick solid lines) and DR (thin solid lines) models. The curves correspond, from top to bottom, to ϕ_F values of 0 (interstellar), 350, 550 and 1000 MV. (b) The expected spectra for the secondary $\bar{p}$ (SLB) only (solid lines), secondary $\bar{p}$ (SLB) plus $\bar{p}$'s from evaporating PBHs (dashed lines), and secondary $\bar{p}$ (SLB) plus $\bar{p}$'s from neutralino annihilation (dotted lines). The upper and lower curves correspond to ϕ_F = 350 and 1000 MV respectively. The normalization parameters for the primary sources are the same as in (a). Also shown is the expected statistical accuracy of a future observation [12]. (c) Same as (b) with the DR model of the secondary $\bar{p}$'s.

↓
factor 3
↑

neutralino

$m_\chi \simeq 50$ GeV

$\frac{\text{solar min}}{\text{solar max}} \sim 3$

$\frac{\text{solar min}}{\text{solar max}} \sim 1.2$ for secondary $\bar{p}$

Bergstrom, Edsjö & Ullio
Astro-ph/9902012

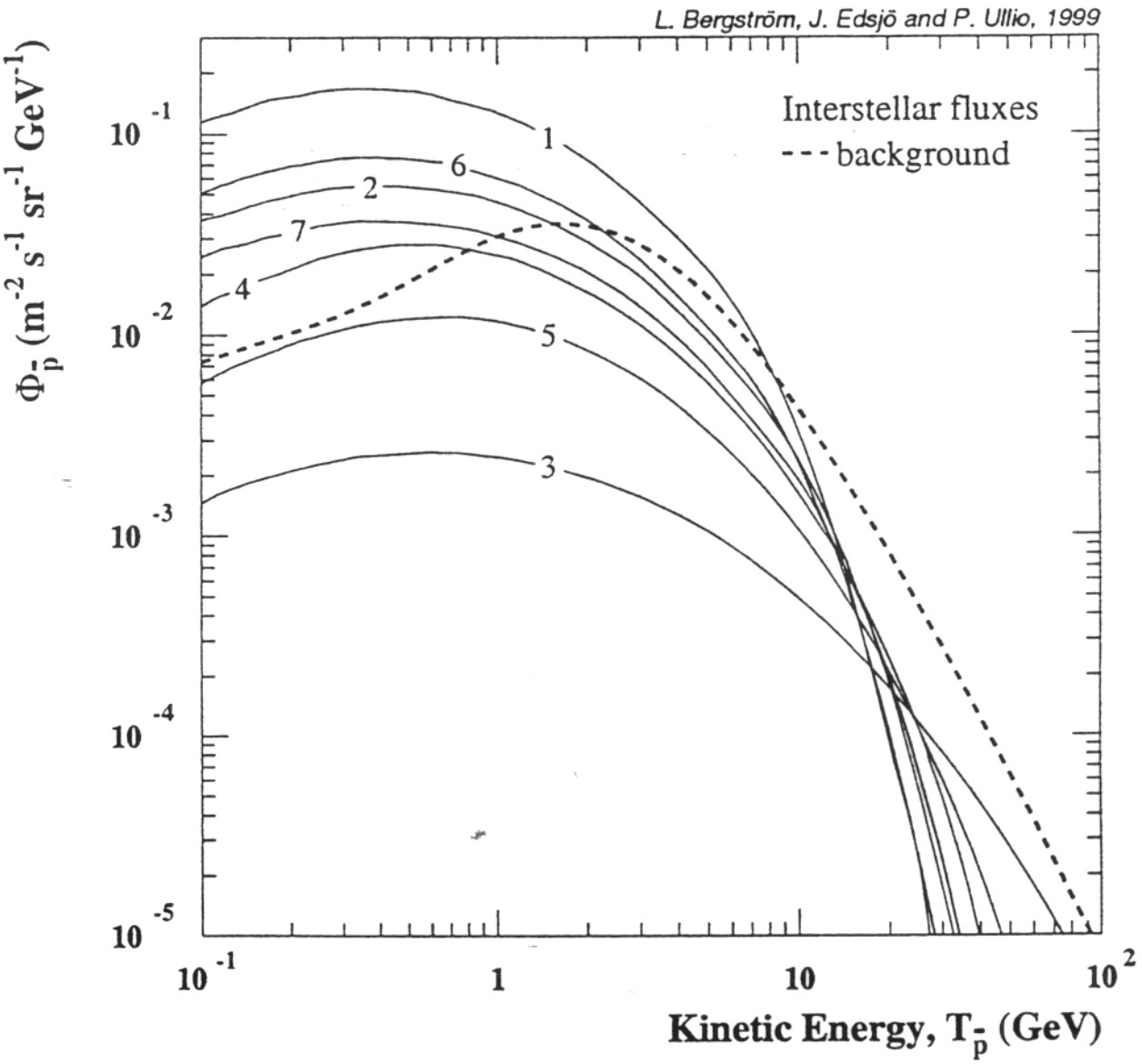

$\frac{min}{max} \cong 1.9$ neutralino, $M_X \sim 100$ GeV

$\frac{min}{max} \cong 1.4$ secondary $\bar{p}$

BESS S. Orito, H. Matsunaga et al.

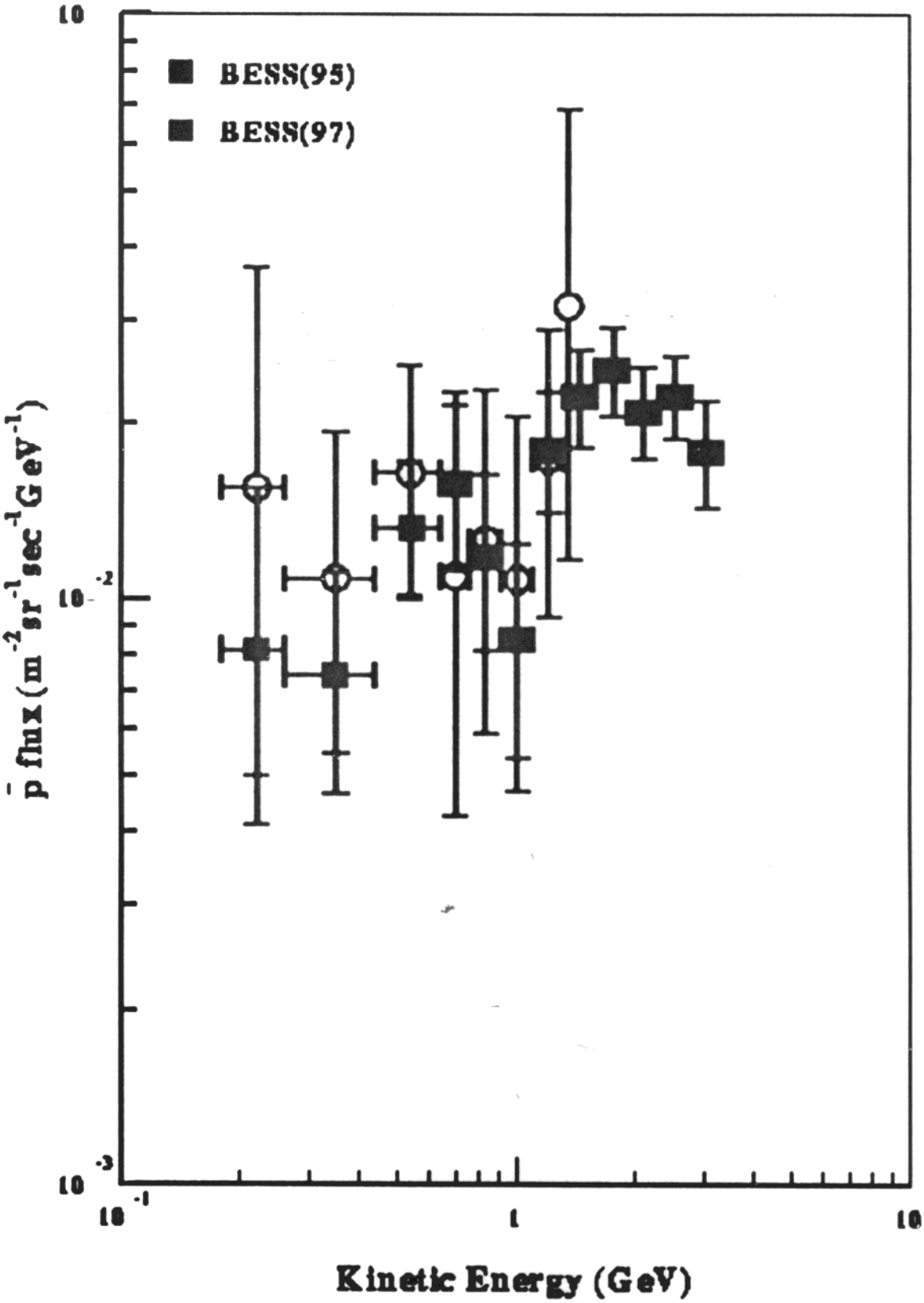

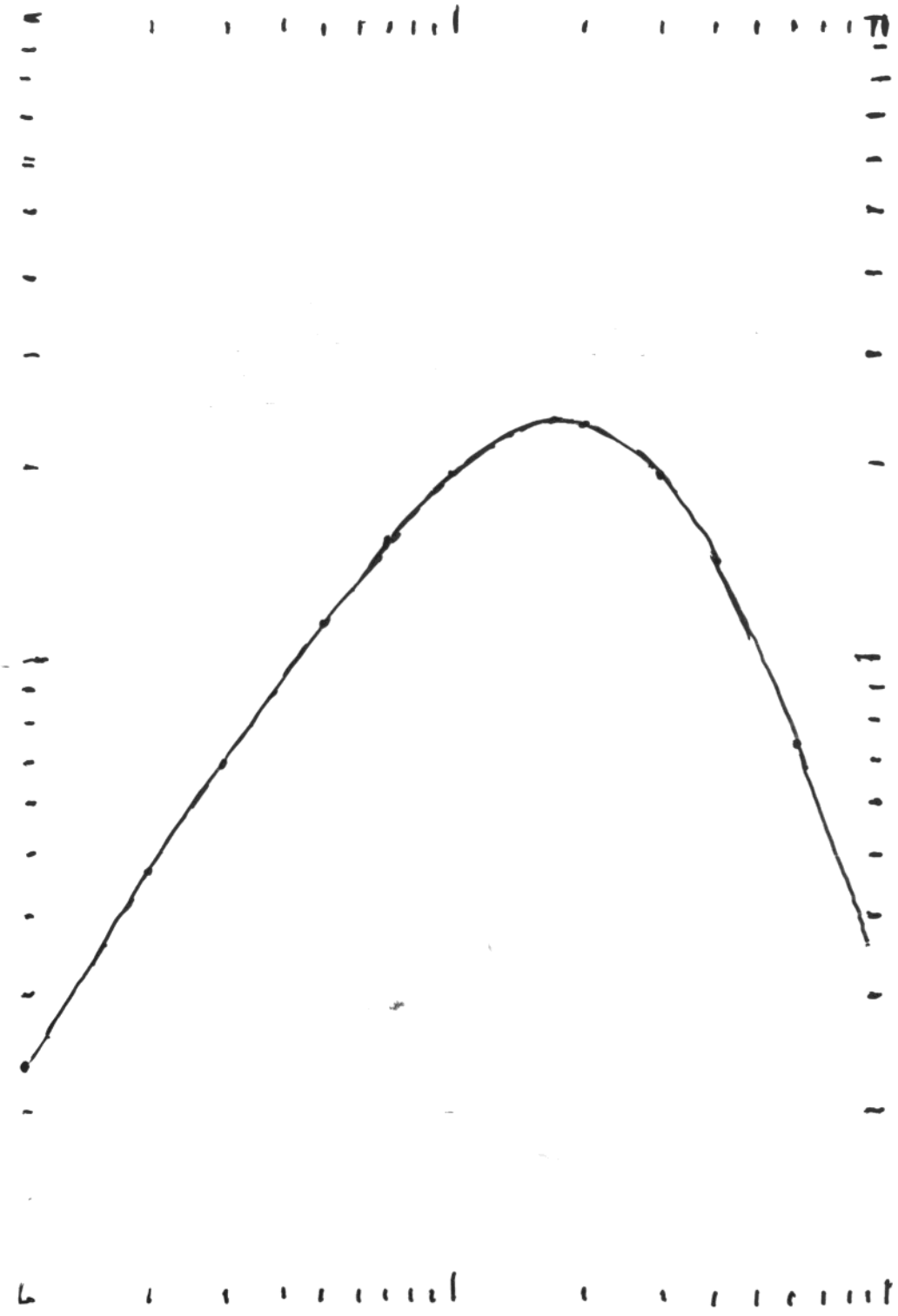

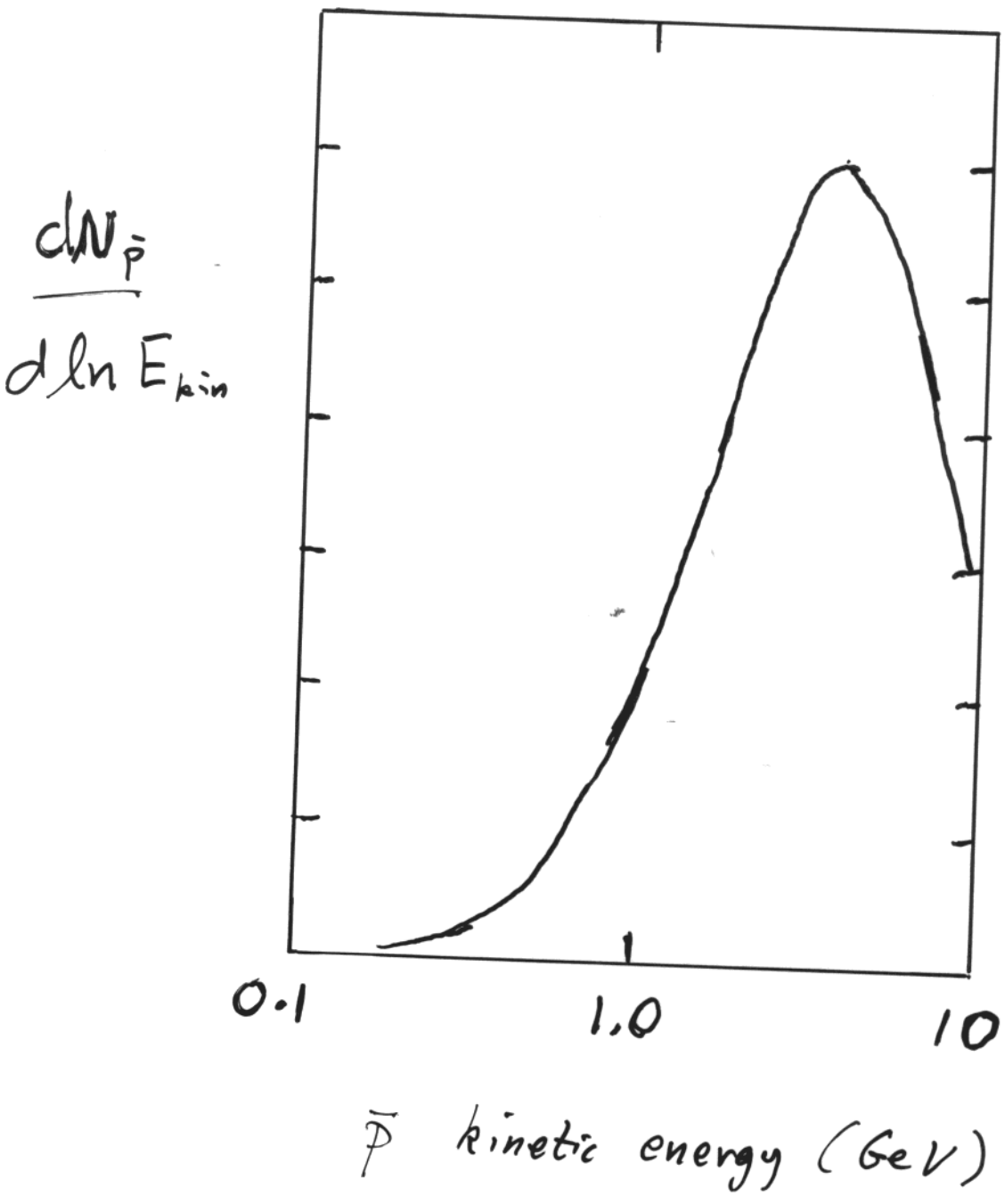
$\frac{dN_{\bar{p}}}{d \ln E_{kin}}$
0.1
1.0
10
$\bar{p}$ kinetic energy (GeV)

Thanks to John Bieber

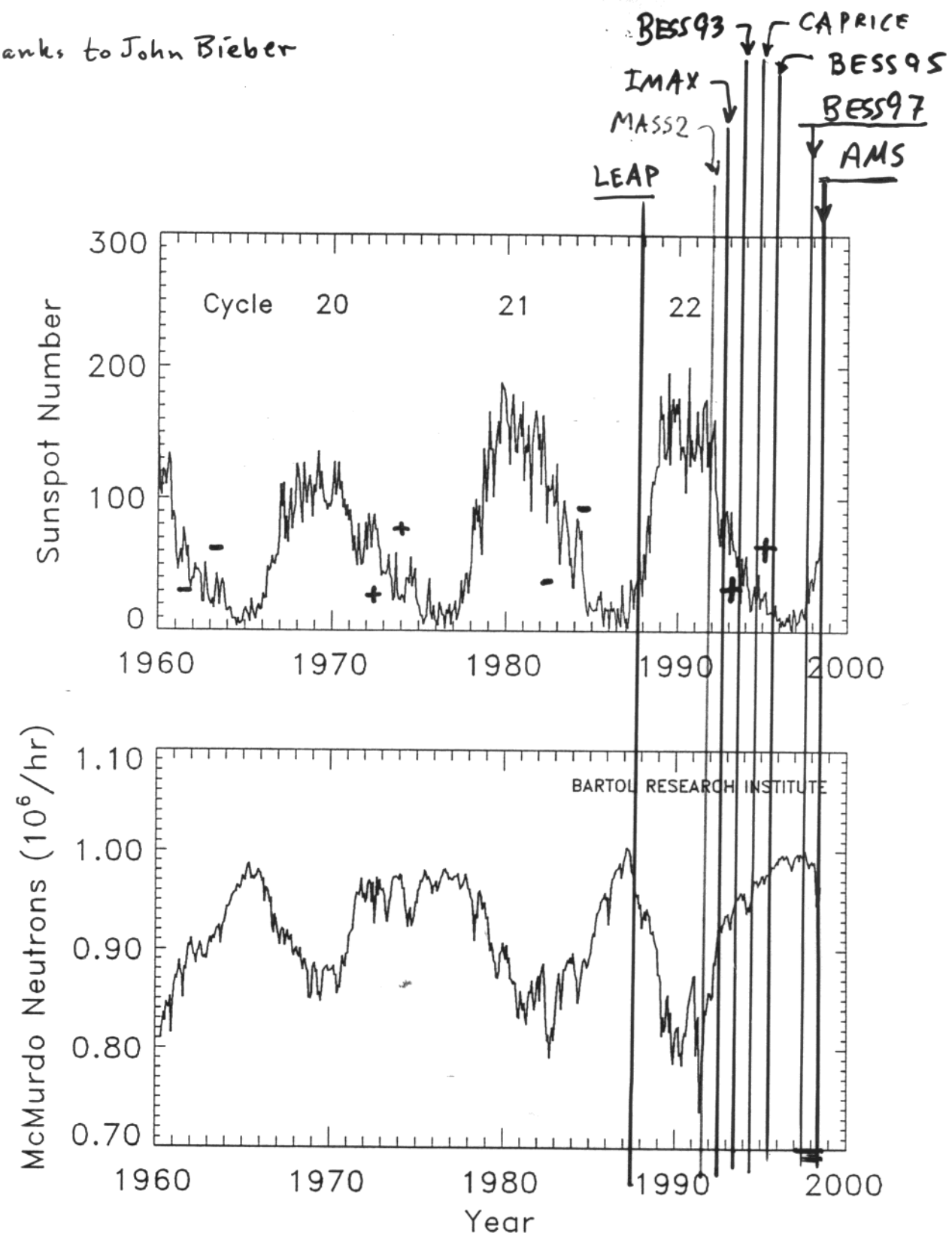

from M. Longair, High Energy Astrophysics vol 1
Cambridge 1992

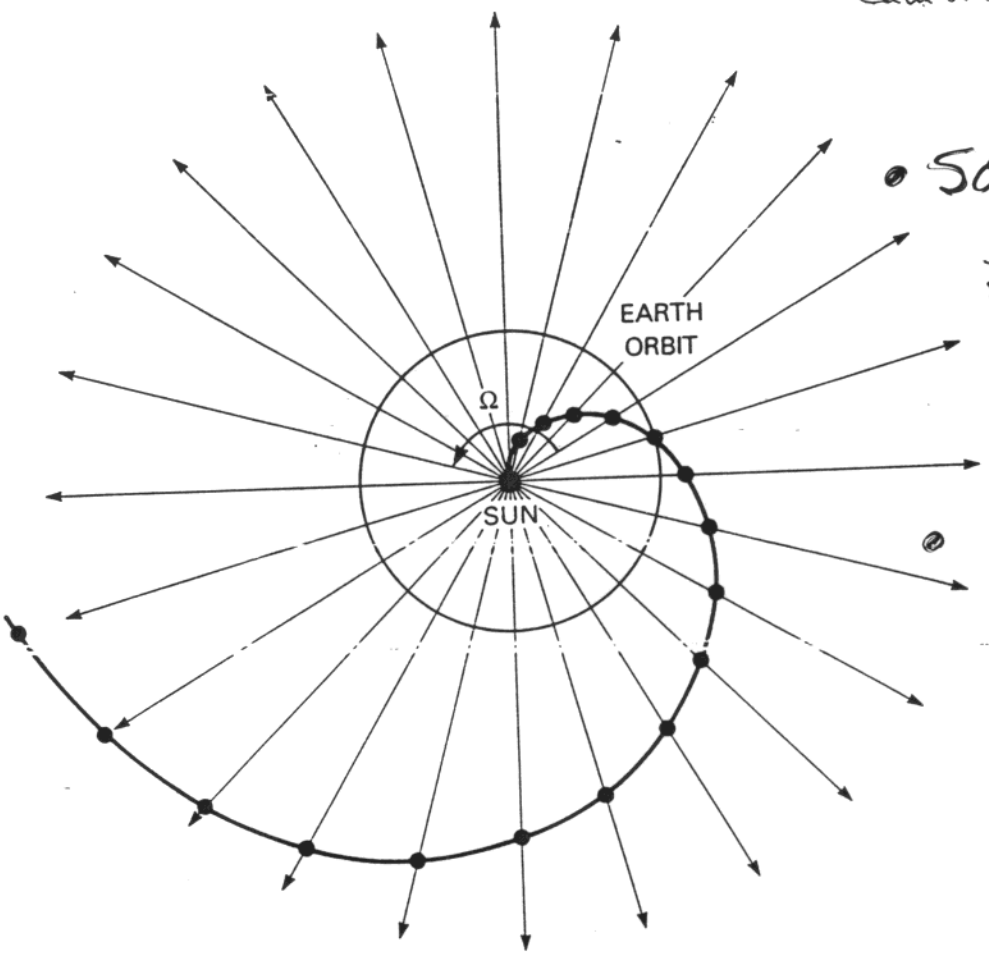

(a)

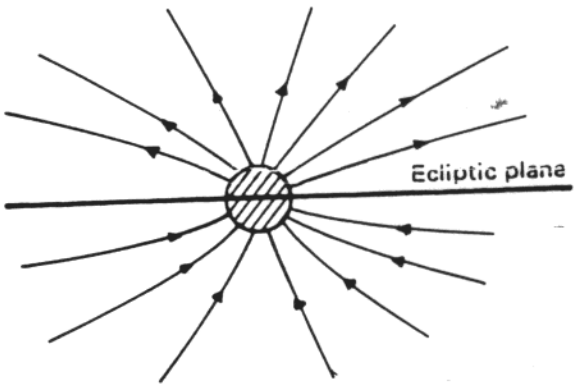

(b)

- Solar wind
  ≳ 400 km/s
  to ≳ 60 AU
- Level of turbulence (scattering) changes from Solar max to Solar min
- 22 yr cycle
  - $B_\odot$ reverses in 11 yr cycles
- Solar max ~ reversal

Figure 10.7. (*a*) A schematic diagram showing how the magnetic field of the Solar Wind takes up a spiral configuration. The plasma leaving the solar corona moves out more or less radially and the magnetic field is dragged with it. The diagram shows the dynamics of plasma associated with one field line while the Sun rotates through half of one rotation. At large distances, the spiral is Archimedean.
(*b*) A schematic diagram showing the structure of the magnetic field out of the plane. The magnetic field has opposite polarity on either side of the neutral sheet.

Drift pattern of + particles

in A^+  solar B field

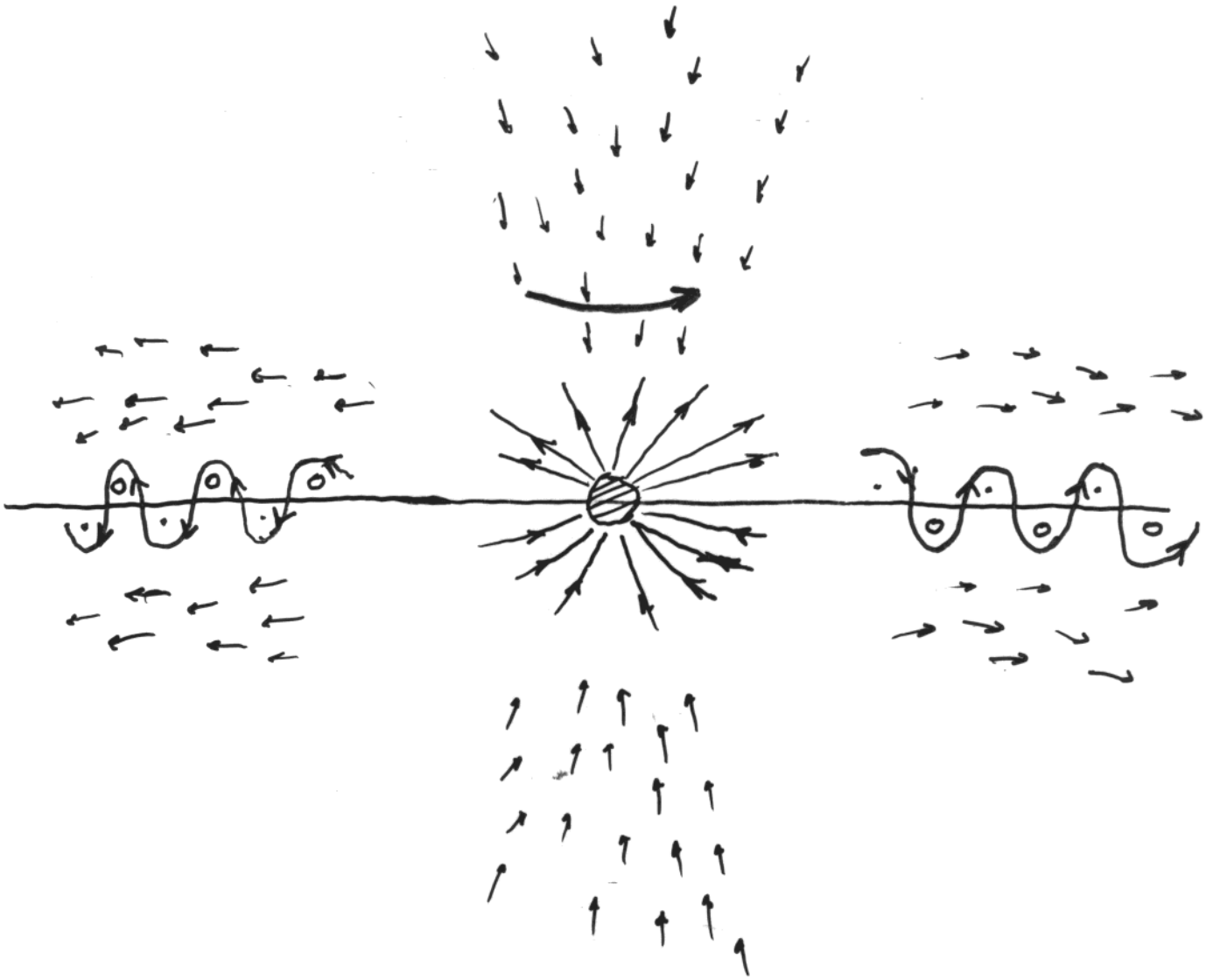

When tilt of current sheet is large (near solar max)

less modulation of positive } particles in A^+
more modulation of negative }

1999-2000
$\bar{p}/p$ small

vice versa in A^-

2000-2001
$\bar{p}/p$ large

Figure 10.8. (a) A schematic diagram showing the sector structure observed in the magnetic field distribution in the Solar Wind when the field direction is measured close to the plane of the ecliptic. (After J. M. Wilcox and N. F. Ness (1965). J. Geophys. Res., **70**, 5793.)
(b) A model of the wavy inclined neutral sheet (or heliospheric current sheet) which separates the opposite polarities of the magnetic field in the northern and southern halves of the Solar Wind. The sheet is as observed from 30° above the equatorial plane at a distance of 75 AU. The figure is 25 AU across. (From J. R. Jokipii and B. T. Thomas (1981). Astrophys. J., **243**, 1115.)

Since the magnetic field of the Sun is dipolar, we would expect the polarity of the magnetic field to differ on either side of the plane of the ecliptic as illustrated in Figure 10.7(b). The magnetic field distribution in the interplanetary medium was found to have this basic spiral configuration by Wilcox and Ness (1965) but they also found that the magnetic field direction reversed so that, in some sectors, the magnetic field points inwards and in others outwards as indicated schematically in Fig. 10.8(a). It was subsequently noted, however, that the sector structure could equally well be accounted for if the basic north–south polarity of the Solar

CURRENT SHEET AT LARGE TILT ANGLES

A. Bünger see Ap. J. 505 (1998) 244

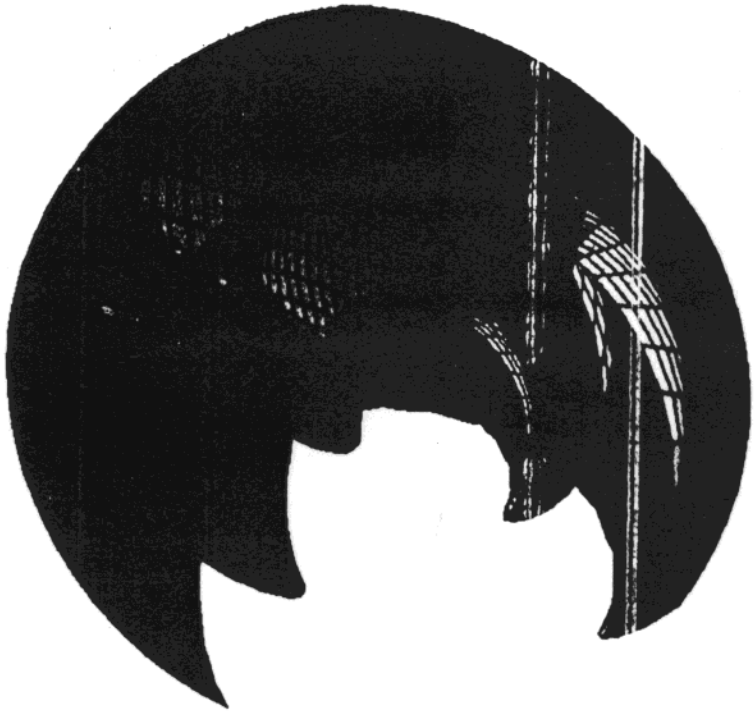

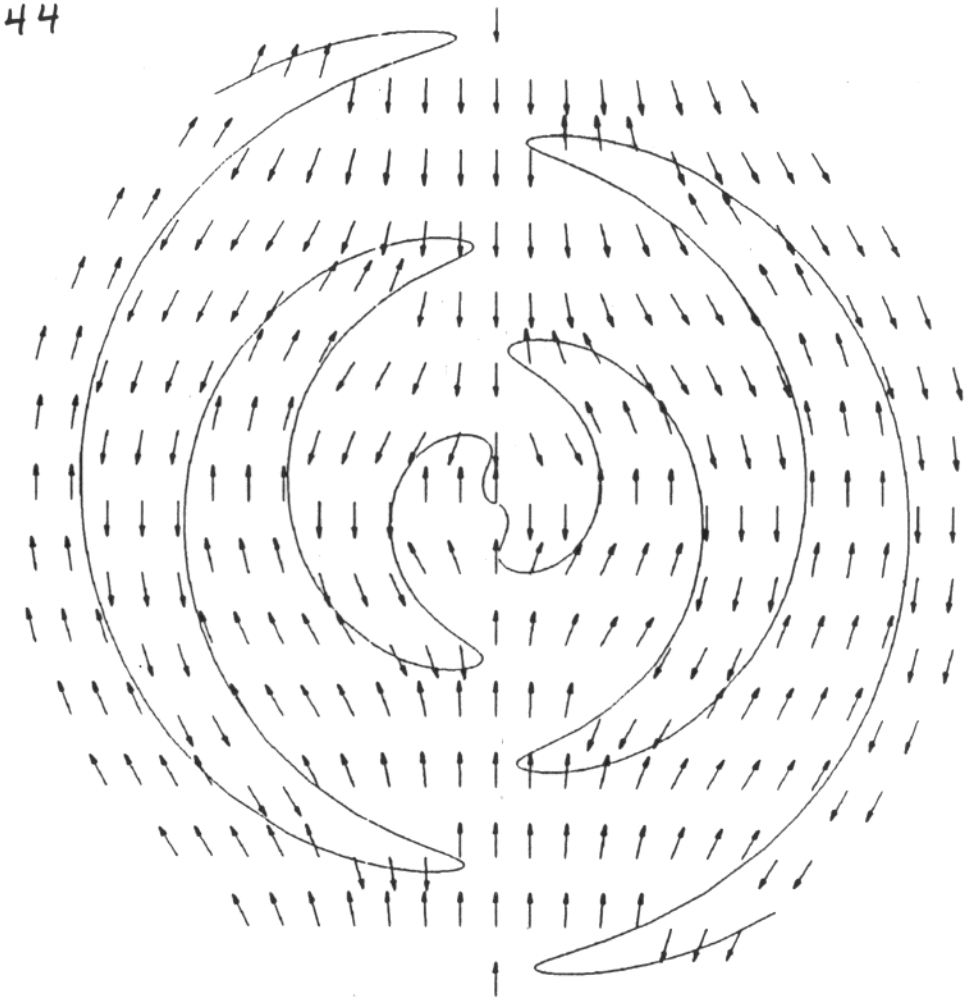

Figure 1: *Left panel shows a cut-away of the wavy current sheet (45° tilt angle and 15 AU radius). Right panel shows drift directions for positively charged particles in an A > 0 cycle (8.5° tilt angle and 15 AU radius).*

Solve transport Eq. for $f(p, \vec{r})$: Burger & Hattingh Ap.J. 505 (199? p.244

$$\vec{\nabla} \cdot (\overleftrightarrow{K} \cdot \vec{\nabla} f) - \vec{V}_w \cdot \vec{\nabla} f + \frac{1}{3} \vec{\nabla} \cdot \vec{V}_w \frac{\partial f}{\partial \ln p}$$

$\phi_p \propto E_p f$

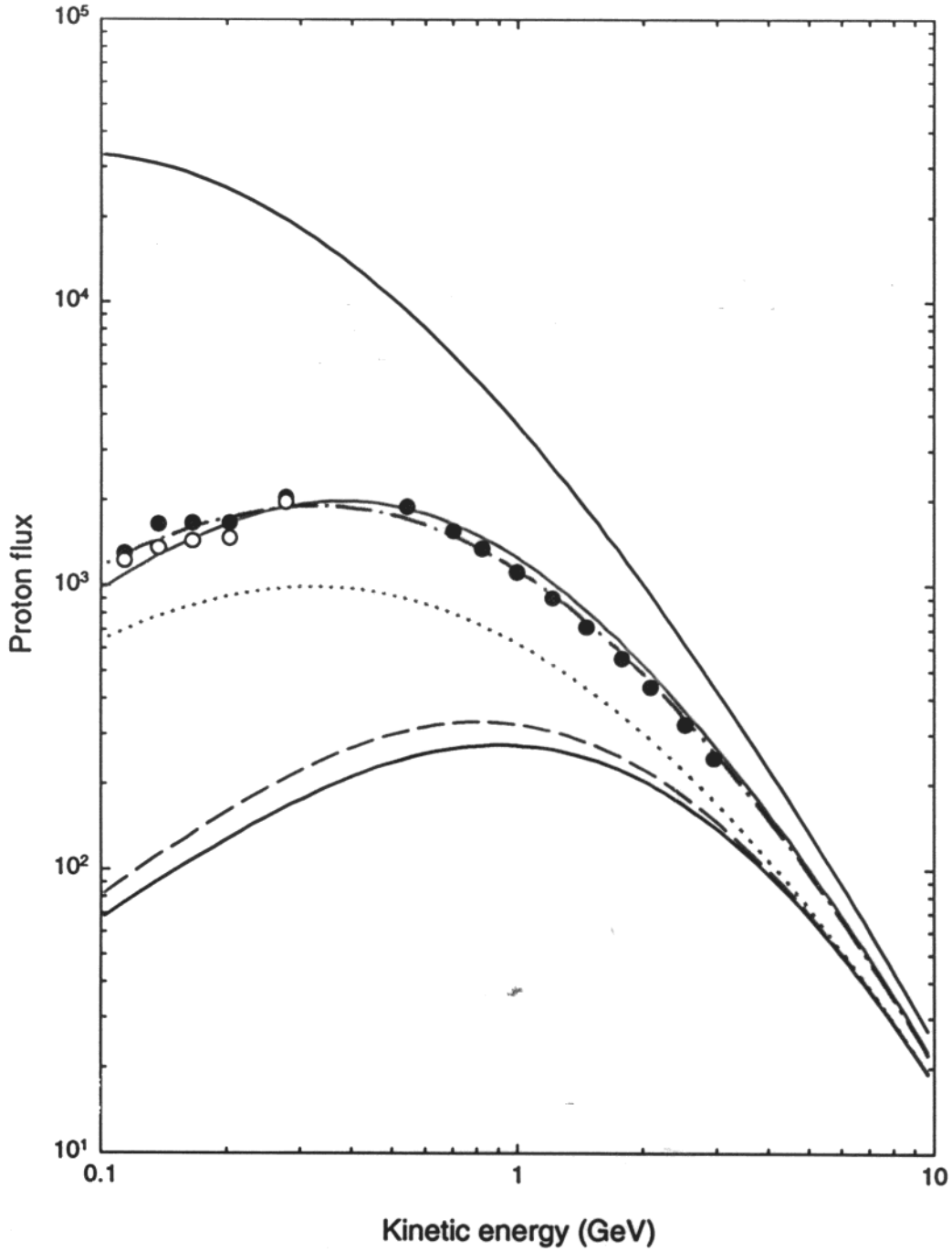

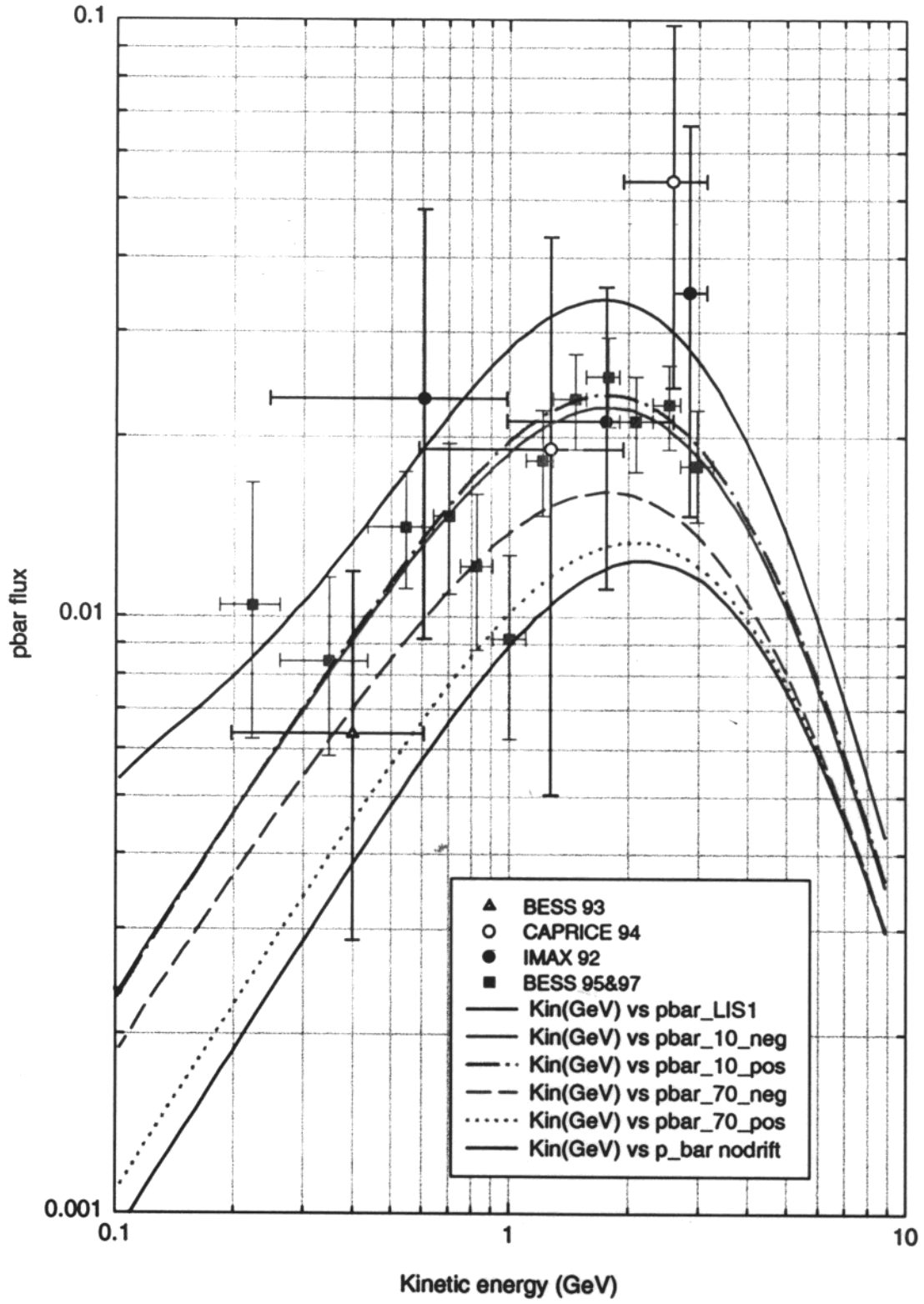
0.1
0.01
0.001
pbar flux
0.1
1
10
Kinetic energy (GeV)
BESS 93
CAPRICE 94
IMAX 92
BESS 95&97
Kin(GeV) vs pbar_LIS1
Kin(GeV) vs pbar_10_neg
Kin(GeV) vs pbar_10_pos
Kin(GeV) vs pbar_70_neg
Kin(GeV) vs pbar_70_pos
Kin(GeV) vs p_bar nodrift

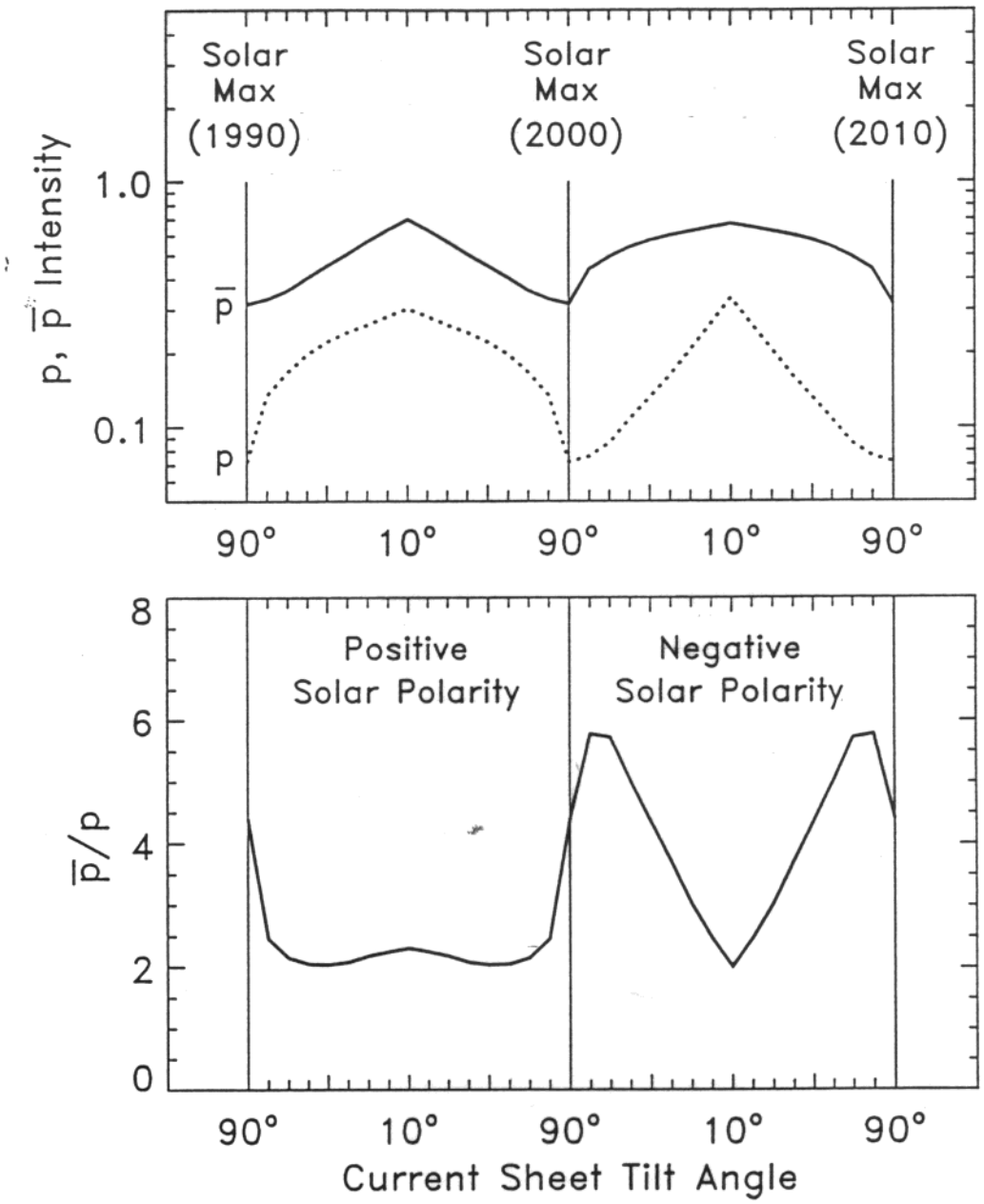
Solar Max (1990)
Solar Max (2000)
Solar Max (2010)
p, p̄ Intensity
1.0
0.1
p̄
p
90°
10°
90°
10°
90°
Positive Solar Polarity
Negative Solar Polarity
p̄/p
8
6
4
2
0
90°
10°
90°
10°
90°
Current Sheet Tilt Angle

Fig. 2

Summary

- After solar max (2000-2002)
  $\bar{p}$ flux should recover quickly
  proton flux slowly in $\leq$ GeV region

- Any low E primary component
  would be a quantitative effect
  (no spectral signature)
  superimposed on this